Chinese Chemical Letters 37 (2026) 112408

Contents lists available at ScienceDirect

Chinese Chemical Letters

journal homepage: www.elsevier.com/locate/cclet

Multiscale engineering for regulating oxygen reduction activity in direct methanol fuel cell: A review

Shiquan Guo[a,*], Fei Chen[b], Congju Li[b,c,*]

[a] School of Materials Science and Engineering, North China University of Water Resources and Electric Power, Zhengzhou 450045, China
[b] School of Energy and Environmental Engineering, University of Science and Technology Beijing, Beijing 100083, China
[c] College of Textiles, Donghua University, Shanghai 201620, China

ARTICLE INFO

Article history:
Received 16 June 2025
Revised 13 December 2025
Accepted 12 January 2026
Available online 13 January 2026

Keywords:
Oxygen reduction reaction
Electrocatalysts
Modification strategies
Electrocatalytic performance
Direct methanol fuel cell

ABSTRACT

Direct methanol fuel cell (DMFC) is a clean energy technology that integrates high-efficiency energy conversion with environmental benefits. However, its industrial application is hindered by the sluggish kinetics of the cathode oxygen reduction reaction (ORR). This key scientific challenge has driven diversified advances in high-performance ORR electrocatalysts. This review systematically outlines the reaction mechanisms and ORR pathways in DMFC. Furthermore, it comprehensively summarizes recent advances in multi-scale modification strategies, including methanol tolerance optimization, rational design of active sites, electronic structure tailoring, surface/interface micro-environment engineering, and additional modulation approaches for enhancing ORR performance. Additionally, the mechanisms for enhancing intrinsic catalytic activity are discussed in depth, along with the elucidation of the structure-activity relationship governing catalyst performance in terms of activity, selectivity, and stability. Finally, in light of the critical challenges currently facing DMFC cathode catalysts, future directions and development pathways for catalyst design are proposed.

© 2026 Published by Elsevier B.V. on behalf of Chinese Chemical Society and Institute of Materia Medica, Chinese Academy of Medical Sciences.

1. Introduction

Energy crisis and climate change are two major challenges facing humanity. Currently, fossil fuels continue to dominate the energy landscape in the near to medium term, exacerbating issues of severe energy shortage and environmental pollution [1,2]. These challenges have raised concerns regarding energy security and environmental sustainability. Guided by the "dual carbon" strategy, establishing a clean energy system is essential for effective resource integration and sustainable energy development [3–5]. To date, multiple energy storage and production technologies based on renewable energy sources have been developed, including hydrogen energy [6], solar power [7], wind energy [8], biomass energy [9], secondary batteries [10], and fuel cell [11]. Among them, the direct methanol fuel cell (DMFC) stands out due to its high energy density (4780 Wh/L), rapid cold-start capability, high conversion efficiency, clean and environmentally friendly fuel, and superior safety features [12–15]. Regarded as a highly promising power generation technology, DMFC is positioned to play a key role in the fast-growing portable electronics market, including laptops, smartphones, and similar devices [16–18]. Liquid methanol offers notable advantages in storage and transport compared to other fuel. Moreover, as methanol can be synthesized from CO_2, making it a target product of the "liquid sunshine" initiative, it not only supports economic growth by resource recycling but also helps mitigate the shortage of liquid fuels [19,20].

Structurally, the DMFC comprises an external circuit, ion-exchange membrane, gas diffusion layers, bipolar plates, and catalyst-based electrodes. Fig. 1 schematically illustrates the principles of both acidic and alkaline DMFC systems. In an acidic medium, methanol solution is delivered to the anode through flow channels and oxygen to the cathode. Methanol oxidation reaction (MOR) at the anode produces protons, electrons, and carbon dioxide. The protons migrate through the membrane to the cathode, while electrons travel *via* the external circuit, where they combine with oxygen to form water (Fig. 1a). In alkaline DMFC, oxygen reduction at the cathode generates hydroxide ions, which migrate through the anion exchange membrane to the anode and react with methanol, producing carbon oxides (Fig. 1b). The circuit completes the energy loop, powering external loads. DMFC directly converts the chemical energy of methanol into electricity, circumventing the Carnot cycle limitation, thereby achieving higher efficiency [21]. The thermodynamic cell potential is 1.21 V at 25 °C.

* Corresponding authors.
E-mail addresses: gasongsq@163.com (S. Guo), congjuli@126.com (C. Li).

https://doi.org/10.1016/j.cclet.2026.112408
1001-8417/© 2026 Published by Elsevier B.V. on behalf of Chinese Chemical Society and Institute of Materia Medica, Chinese Academy of Medical Sciences.

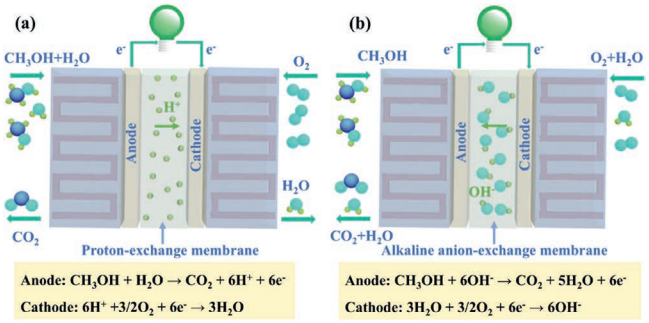


Fig. 1. (a, b) Schematic diagram of DMFC in acidic and alkaline media.

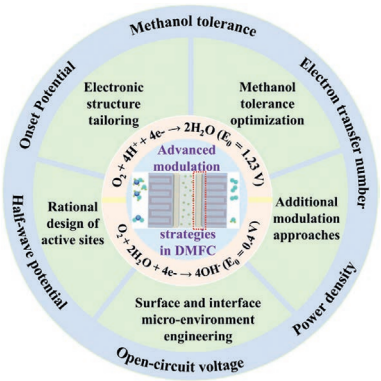


Fig. 2. Modification strategies for cathode electrocatalysts in DMFC.

However, the actual voltage and power output are considerably lower due to polarization loss, mixed potential, catalyst poisoning, electrode kinetics limitation, operating condition, and material degradation [22,23]. A major factor limiting performance is the sluggish oxygen reduction reaction (ORR) kinetics at the cathode, where currently available electrocatalysts remain a critical bottleneck [24,25].

In fuel cell, the ORR at the cathode necessitates a high overpotential to overcome kinetic energy barrier. Therefore, the development of highly active and stable ORR catalysts has become a major research focus in the field [26–29]. An ideal cathode electrocatalyst for DMFC should possess the following features: (1) High specific surface area and rich pore structure to expose abundant active sites and facilitate the adsorption and diffusion of reactants; (2) High catalytic activity to lower the activation energy and promote ORR kinetics; (3) Good conductivity to enable efficient electron transfer; (4) Strong tolerance to methanol crossover to suppress MOR; (5) High chemical stability to prevent material degradation or failure. Significant progresses have been made in catalysts design in recent decades, driven by advances in structural innovation, nanoengineering, and advanced characterization techniques [30–32]. Among various catalysts, Pt/C remains the most active ORR electrocatalyst for metal air cells and fuel cells, despite the high cost and limited stability. However, CO poisoning is prone to occur due to the methanol crossover effect in DMFC, which deactivates catalytic sites [33,34]. Studies have shown that optimizing the surface properties and atomic arrangement of Pt-based materials is crucial for improving both durability and methanol tolerance [35–37]. Surface modification has emerged as an effective strategy to enhance ORR performance. Non-precious metal-based catalysts have also attracted attention due to their inherent methanol tolerance. Nevertheless, the catalytic activity remains inferior to that of commercial Pt/C. Enhancing the performance of such materials, particularly through systematic multi-scale engineering strategies for catalyst modification, represents a critical research challenge [38,39].

This review is organized as follows: First, the working mechanisms of DMFC in acidic and alkaline environments are briefly discussed. Then, the kinetic mechanisms of the ORR and commonly used electrochemical evaluation methods are introduced. Subsequently, recent advances in multi-scale modulation strategies for enhancing ORR activity are systematically reviewed, including methanol tolerance optimization, rational design of active sites, electronic structure tailoring, surface/interface micro-environment engineering, and additional modulation approaches (Fig. 2). A detailed discussion is provided from multiple perspectives, including core-shell structures, crystal facet control, surface modification, confinement effects, coordination environment optimization, doping strategies, alloying, heterostructure construction, pore structure design, hydrophilicity/hydrophobicity regulation, composition and size control, and defect engineering. These strategies are examined across advanced material systems such as precious metal-based catalysts, carbon-based materials, single-atom catalysts, alloy catalysts, and metal oxides. Furthermore, the structure-activity relationships are emphasized, and the corresponding catalytic mechanisms are comprehensively analyzed. Finally, the remaining challenges and future development directions for DMFC catalysts are outlined.

2. Fundamental understanding of ORR mechanism

ORR is considered one of the essential electrocatalytic reactions in energy storage and conversion systems, unraveling the intrinsic mechanism of ORR is crucial for the rational design and selection of electrocatalysts with tailored structures and properties [40,41]. The reaction primarily involves three steps: (1) Adsorption of O_2 on the catalyst surface; (2) Electron transfer and O_2 reduction; (3) Desorption of reduction products. These processes involve the adsorption and desorption of oxygen-containing intermediates, cleavage and formation of chemical bonds, as well as protons and electrons transfer [42]. The adsorption of O_2 on the electrode surface is the initial and rate-determining step of the ORR, making it essential to understand the possible adsorption modes. In general, three distinct adsorption modes are recognized on the catalyst surface, mainly the Pauling model, Bridge model, and Griffiths model, as illustrated in Fig. 3a [43]. In the Pauling model, O_2 is adsorbed in an "end-on" fashion, with one oxygen atom bonds to a single site, this mode weakly perturbs the O–O bond and often leads to the $2e^-$ reduction pathway, producing H_2O_2. Bridge model is known as "side-on" manner, in which both oxygen atoms bond to two adjacent sites and favors the $4e^-$ pathway toward H_2O. In the Griffiths model, the oxygen atoms bound laterally to a single active site. This facilitates O–O bond activation and cleavage, similar favoring the $4e^-$ pathway. In summary, the adsorption mode of O_2 at the active site critically determines the ORR pathway selectivity.

Typically, the ORR typically proceeds *via* either a $4e^-$ pathway to H_2O, which is ideal for fuel cells and metal-air batteries, or a $2e^-$ pathway to H_2O_2, which is desirable for environmental remediation and other applications (Eqs. 1–6).

(1) $4e^-$ pathway:

Acid medium:

$$O_2 + 4H^+ + 4e^- \rightarrow 2H_2O,\ E^0 = 1.229\ V \quad (1)$$

Alkaline medium:

$$O_2 + 2H_2O + 4e^- \rightarrow 4OH^-,\ E^0 = 0.401\ V \quad (2)$$

(2) $2e^-$ pathway:

Acid medium:

$$O_2 + 2H^+ + 2e^- \rightarrow H_2O_2,\ E^0 = 0.670\ V \quad (3)$$

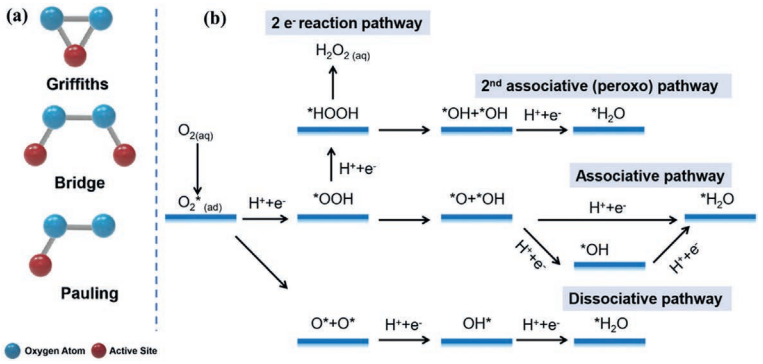


Fig. 3. (a) Different O_2 adsorption modes on the catalytic surface and (b) the ORR reaction pathways *via* $2e^-$ and $4e^-$. Reproduced with permission [43]. Copyright 2024, Royal Society of Chemistry.

$$H_2O_2 + 2H^+ + 2e^- \rightarrow 2H_2O,\ E^0 = 1.770\ V \quad (4)$$

Alkaline medium:

$$O_2 + H_2O + 2e^- \rightarrow OH^- + HO_2^-,\ E^0 = -0.065\ V \quad (5)$$

$$HO_2^- + H_2O + 2e^- \rightarrow 3OH^-,\ E^0 = 0.867\ V \quad (6)$$

The detailed reduction of O_2 to H_2O can be divided into three distinct pathways: Associative pathway (Eqs. 7–11), dissociative pathway (Eqs. 12–14), and 2nd associative pathway (Eqs. 15–19), as shown in Fig. 3b.

(1) Associative pathway:

$$O_2 + * \rightarrow O_2^* \quad (7)$$

$$O_2^* + H^+ + e^- \rightarrow OOH^* \quad (8)$$

$$OOH^* + H^+ + e^- \rightarrow O^* + H_2O \quad (9)$$

$$O^* + H^+ + e^- \rightarrow OH^* \quad (10)$$

$$OH^* + H^+ + e^- \rightarrow H_2O + * \quad (11)$$

(2) Dissociative pathway:

$$O_2 + 2^* \rightarrow 2O^* \quad (12)$$

$$2O^* + 2H^+ + 2e^- \rightarrow 2OH^* \quad (13)$$

$$2OH^* + 2H^+ + 2e^- \rightarrow 2H_2O + 2^* \quad (14)$$

(3) 2nd associative pathway:

$$O_2 + * \rightarrow O_2^* \quad (15)$$

$$O_2^* + H^+ + e^- \rightarrow OOH^* \quad (16)$$

$$OOH^* + H^+ + e^- \rightarrow HOOH^* \quad (17)$$

$$HOOH^* \rightarrow 2OH^* \quad (18)$$

$$2OH^* + 2H^+ + 2e^- \rightarrow 2H_2O + 2^* \quad (19)$$

where * represents an active site on the catalytic surface. The reaction kinetics and pathways of ORR are determined by the adsorption energy of intermediates on the catalyst surface. An ideal catalyst should exhibit moderate adsorption strength toward reaction intermediates. Excessively strong adsorption may occupy active sites and inhibit desorption, impairing reaction continuity, whereas overly weak binding may be insufficient to activate key species [44,45]. Therefore, rational catalyst design, which focuses on optimizing the free energy of oxygen-containing intermediates on catalytic surface sites, is essential for enhancing ORR performance.

To evaluate the ORR catalytic performance, a rotating disk electrode (RDE) or rotating ring-disk electrode (RRDE) is typically employed in combination with an electrochemical workstation. Common electrochemical techniques include cyclic voltammetry (CV), linear sweep voltammetry (LSV), chronoamperometry (CA), and electrochemical impedance spectroscopy (EIS). Key evaluation metrics for catalytic activity comprise the onset potential (E_{onset}), half-wave potential ($E_{1/2}$), electron transfer number, stability, Tafel slope, electrochemically active surface area (ECSA), kinetic current density (J_k), and limiting current density (J_L).

3. Optimization of ORR performance in DMFC by various regulation strategies

The ORR process is fundamentally determined by the electronic structure and physicochemical properties of the catalyst interface, which dictate the adsorption and desorption behavior of oxygen-containing intermediates. To enhance electrocatalytic performance, various strategies, such as heterointerface engineering, defect engineering, composite design, and surface functionalization, have been extensively explored [46–49]. Specific methods like heteroatom doping, size confinement, surface reconstruction, and pore structure control are employed to tailor the electronic environment, morphological features, active sites, and porosity of catalysts, thereby improving reaction kinetics. Ideal catalysts should exhibit high specific surface area, abundant porosity, excellent conductivity, and well-exposed active sites, along with stability in acidic/alkaline environments, resistance to methanol/CO poisoning, and avoidance of mixed potentials [50,51]. In addition to experimental and advanced characterization techniques, theoretical studies play a key role in high-throughput catalyst screening and mechanistic elucidation [52,53]. Establishing a clear structure-performance relationship and understanding how various modification strategies regulate ORR activity are essential for the rational design of efficient DMFC catalysts. Tables S1 and S2 (Supporting information) summarize the recent advances in catalytic materials, highlighting their key electrochemical performance metrics across different media.

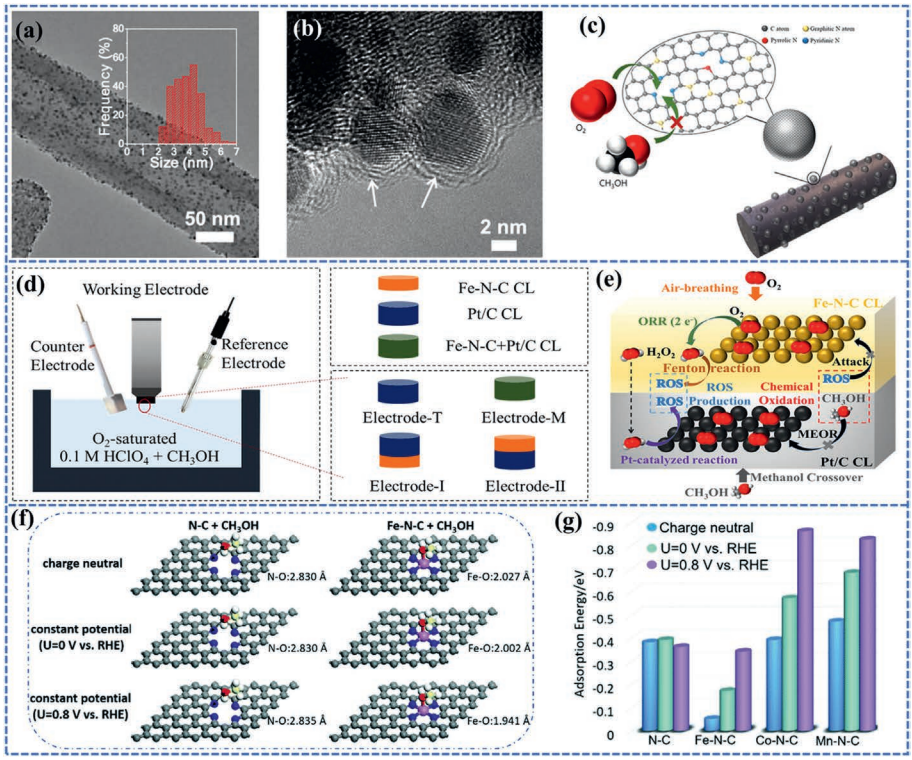


Fig. 4. (a) TEM and (b) HRTEM images of Pt@CS/CNF. (c) Mechanisms of methanol tolerance and enhanced oxygen reduction. Reproduced with permission [61]. Copyright 2020, American Chemical Society. (d) Schematic of electrodes composed of Pt/C and Fe-N-C. (e) Mechanism schematic of DMFC based on composite cathode catalytic layer. Reproduced with permission [64]. Copyright 2024, Elsevier. (f) Adsorption configuration of methanol on N–C and FeN_4 sites obtained by DFT calculations. (g) The adsorption energy of methanol on N–C, FeN_4, CoN_4, and MnN_4 active sites calculated at different potentials. Reproduced with permission [66]. Copyright 2020, Royal Society of Chemistry.

3.1. Methanol tolerance optimization

Precious metal catalysts (such as Pt, Pd) typically exhibit high electrocatalytic activity and are widely used as benchmarks. However, their application in DMFC is limited by methanol crossover poisoning, where methanol permeates from the anode to the cathode through the membrane, severely degrading catalyst performance [23,54]. The development of precious metal-based catalysts aims to simultaneously increase active site density and improve methanol tolerance. Nanostructure engineering and surface modification have been demonstrated to significantly enhance both the catalytic activity and methanol resistance of Pt-based catalysts. Furthermore, the improvement in ORR performance has been attributed to strain effects and multi-component synergy [32,55]. Meanwhile, non-precious metal catalysts typically exhibit intrinsic methanol tolerance, though the catalytic activity still requires further improvement.

DMFC commonly use low-concentration methanol to suppress crossover and sustain performance [23]. However, high methanol concentrations are essential for competitive energy density. To overcome this limitation, Feng *et al.* [56] designed selective electrocatalysts that facilitate operation under high methanol concentrations. The resulting Au@Pd catalyst demonstrated enhanced ORR activity due to Au-Pd synergy, including electronegativity-driven electronic coupling and lattice mismatch-induced strain effects. The assembled DMFC achieved a peak power density of 89.7 mW/cm^2 operating at 80 °C with 10 mol/L methanol aqueous solution, while maintaining high performance even at 15 mol/L. Tetrahedral Pd nanocrystals often show enhanced ORR activity in alkaline media owing to the high surface-to-volume ratio and exposed (111) facets [57]. For instance, Wang *et al.* [58] synthesized uniform truncated Pd tetrahedrons (T-Pd-Ths) enclosed by (111) facets, which feature low-coordination sites and lattice distortion that introduce localized strain. The T-Pd-Ths/C catalyst exhibited specific and mass activities 10.7 and 14.1 times higher than those of commercial Pt/C, respectively, along with high CO tolerance and only 7.69% activity loss after 50,000 cycles. Theoretical simulations confirmed that low coordination sites enhanced ORR performance. A DMFC using T-Pd-Ths/C achieved an open-circuit voltage of 0.927 V and a peak power density of 163.7 mW/cm^2 across tested temperatures. Ultrathin carbon layers can effectively anchor Pt nanoparticles onto carbon supports, suppressing their migration, aggregation, detachment, and dissolution, while also inhibiting methanol penetration [59]. For example, Tong *et al.* [60] developed an *in-situ* polymer nanoencapsulation-graphitization strategy to prepare carbon-coated Pt/CNTs@C catalysts. The carbon layer thickness, adjustable from 0.5 nm to several nanometers *via* controlled polymer growth, was found to critically influence ORR activity. The optimized Pt/CNTs@C exhibited high catalytic activity, durability, and methanol tolerance. In a related approach, Lee *et al.* [61] encapsulated individual Pt nanoparticles within graphitic carbon shells (Pt@CS/CNF). As shown in Figs. 4a and b, transmission electron microscopy (TEM) and high-resolution TEM (HRTEM) images revealed uniformly dispersed Pt nanoparticles (~3.8 nm) within the nanofibers, with the surrounding carbon shell effectively preventing aggregation. The carbon shell significantly blocked methanol access to the Pt core, an effect enhanced by higher graphitization, while still permitting O_2 permeation to facilitate the ORR process (Fig. 4c).

To address the trade-off between oxygen catalytic activity and poisoning tolerance, Zhang *et al.* [62] successfully synthesized a class of Pd-Te hexagonal nanoplates (Pd-Te HPs) featuring a $Pd_{20}Te_7$ phase. Atomic force microscopy (AFM) image showed that the Pd atoms deviated from the hexagonal close-packed arrange-

ment, resulting in exposed bridge sites that serve as catalytic centers. The Pd-Te HPs/C catalyst demonstrated superior ORR activity with $E_{1/2}$ of 0.90 V, long-term stability (retaining 65 % activity after 50,000 s), and exceptional methanol tolerance. Density functional theory (DFT) calculations revealed that the enhanced activity originates from the breakthrough in the linear relationship between OOH* and OH* adsorption, while the MOR remained highly endothermic. Among strategies to mitigate methanol crossover, structural modifications of the membrane electrode assembly (MEA) have shown promising results. For example, Kim *et al.* [63] designed a hierarchically structured cathode with an inner Pt-black layer to shield active sites from methanol and an outer Pt/C layer to enhance the electrochemical active surface area. This graded structure mitigates methanol crossover by enhancing ORR activity. Inspired by the Fenton activity of Fe-N-C, Hou *et al.* [64] systematically optimized electrochemical performance using composite cathode architectures (Fig. 4d). The best cell configuration composed of a layered cathode with Pt/C outside and Fe-N-C inside achieved a peak power density of 24.55 mW/cm^2 with 3 mol/L methanol solution at 30 °C. As illustrated in Fig. 4e, the Fe-N-C layer produced H_2O_2 *via* the 2e$^-$ pathway, which was then decomposed by both Fe-N-C (Fenton reaction) and Pt/C, generating reactive oxygen species (ROS). These ROS may chemically oxidize methanol that crosses over from the anode, suppressing its electrochemical oxidation on Pt and thus preserving cell performance.

To address the issues of high methanol permeability and low conductivity in polymer electrolyte membranes, Tan *et al.* [65] proposed a novel strategy employing methanol-tolerant $NiCo_2O_4$ cathode catalysts combined with a permeable polymer fiber membrane to improve DMFC performance. LSV and *CA* tests indicated that the $E_{1/2}$ of $NiCo_2O_4$ was comparable to commercial Pt/C catalysts, alongside significantly enhanced methanol tolerance. The permeable polymer fiber membrane-based DMFC achieved a maximum power density of 126.2 mW/cm^2 at 60 °C. Shi *et al.* [66] systematically investigated the adsorption behavior of methanol on various active sites at $U = 0$ and 0.8 V *vs.* reversible hydrogen electrode (RHE) using stable adsorption modes (Fig. 4f). Results showed that methanol adsorption strength on MN_4 sites (M = Fe, Co, Mn) correlates strongly with electrode potential, especially at higher potentials (Fig. 4g). Importantly, methanol adsorption neither disrupts the structure of FeN_4 sites nor interferes with the 4e$^-$ ORR pathway. Leveraging this intrinsic methanol tolerance, an atomically dispersed Fe/Co-N-C catalyst through a Co-doping and Fe-adsorption strategy was synthesized. Co was found to modulate pore structure and generate defects for anchoring FeN_4 sites. The resulting DMFC, operating in a methanol-air system, achieved a peak power density of 135 mW/cm^2 using 1 mol/L methanol solution. This work offers a new approach to designing dual-site catalysts with high activity and superior methanol tolerance.

Currently, although modification strategies for precious metal catalysts, such as core-shell structures, high-index facet exposure, surface modification, selective catalytic layers, and functionally graded electrode design, can partially mitigate the methanol crossover effect, it remains challenging to achieve both high ORR activity and ideal methanol tolerance simultaneously. While non-precious metal catalysts exhibit inherent methanol tolerance, the ORR activity still significantly lags behind that of precious metal benchmarks. Consequently, the development of novel catalyst systems that combine high activity and strong tolerance continues to pose a persistent challenge [67,68].

3.2. Rational design of active sites

Rational modulation at the atomic/molecular level enables the precise construction of active centers with tailored geometric configurations, electronic structures, and micro-environments, thereby facilitating directed optimization of catalytic activity, selectivity, and stability. In electrocatalysis, the evolution of active sites from the nanoscale to the single-atom level induces significant changes in geometric and electronic structures, leading to distinct catalytic behaviors. Atomically dispersed catalysts, typically consisting of metal sites anchored atomically on carbon supports, have attracted extensive research interest due to the 100 % atom utilization efficiency [69–71]. Among them, M-N-C materials (M = Fe, Co, Ni, *etc.*), formed by embedding transition metal centers into N-doped carbon matrices, have been widely demonstrated to derive the high ORR activity primarily from the metal sites atomically dispersed and coordinated with N atoms [72,73]. Thus, M-N-C materials are emerging as a mainstream direction in the design and fabrication of ORR catalysts.

Currently, Fe-N-C is evolving into one of the most representative M-N-C materials in DMFC due to its exceptional catalytic efficiency and intrinsic tolerance to methanol/CO poisoning [74–77]. Recent studies show that the confinement engineering based on metal-organic framework (MOF) can stabilize single atoms *via* spatial site isolation to prevent particle agglomeration. Moreover, such confinement engineering readily modulates the coordination environment and electronic structure of active sites *via* chemical bonding, thereby conferring enhanced catalytic activity [78,79]. Xu *et al.* [80] reported an atomically dispersed ZIF/MIL-10–900 catalyst with FeN_4 configuration derived from a MOF mixture of institute lavoisier-101 (MIL-101) and zeolite imidazolate frame-8 (ZIF-8), which enabled the DMFC to achieve an enhanced peak power density of 83 mW/cm^2 operating with 3 mol/L methanol solution at 80 °C. The discrete distribution of active sites necessitates multiscale pore structures to ensure accessibility and efficiency. Shi *et al.* [81] constructed a hierarchically porous FeNC-DT catalyst with smooth morphology *via* a dual-template strategy. The as-prepared catalyst demonstrated a remarkable $E_{1/2}$ of 0.954 V and low Tafel slope of 49.3 mV/dec in alkaline media. To tackle the challenges of insufficient active sites and restricted mass transport at triple-phase boundaries, Shu *et al.* [82] innovatively designed a core-shell structured Fe-mPDA@HPCS catalyst, which consists of hierarchically porous carbon spheres (HPCS) as the core and single-Fe-atom-modified m-phenylenediamine (Fe-mPDA) as the shell. By precisely engineering the pore architecture and strategically incorporating atomic Fe sites (Fig. 5a), the catalyst synergistically enhanced both ORR activity and mass transfer capability.

Previous studies indicate that the suboptimal adsorption energy of oxygen intermediates, induced by the four symmetric electronegative N atoms surrounding Fe centers, fundamentally restricts the catalytic activity of Fe-N-C materials. Notably, partial substitution of N with heteroatoms through secondary coordination engineering has proven effective in modulating electronic structures and enhancing reaction kinetics [83,84]. Cui *et al.* [85] utilized trithiocyanuric acid (TCA)-coated ZIF-8 as precursor to synthesize a hollow porous Fe, N, S-codoped carbon catalyst (Fe/NS-C). In this system, TCA simultaneously enhances N content and introduces S as a secondary dopant, thereby not only providing abundant anchoring sites for Fe single atoms but also modulating the electronic structure. The catalyst features active sites with FeN_4 and FeN_3S coordination configurations (Fig. 5b). Owing to the high intrinsic catalytic activity of FeN_3S sites and the fully exposed active surfaces, the Fe/NS-C material delivered exceptional ORR performance with a $E_{1/2}$ of 0.893 V and J_k of 41.18 mA/cm^2, superior to commercial Pt/C (Fig. 5c).

The suboptimal binding strength of reaction intermediates significantly impedes the ORR kinetic. Although dual-site catalytic mechanism can partially alleviate this limitation by synergistically facilitating oxygen dissociation and O–O bond cleavage, the precise control over the geometric and electronic structures of these dual sites that determine catalytic efficiency remains a fundamental

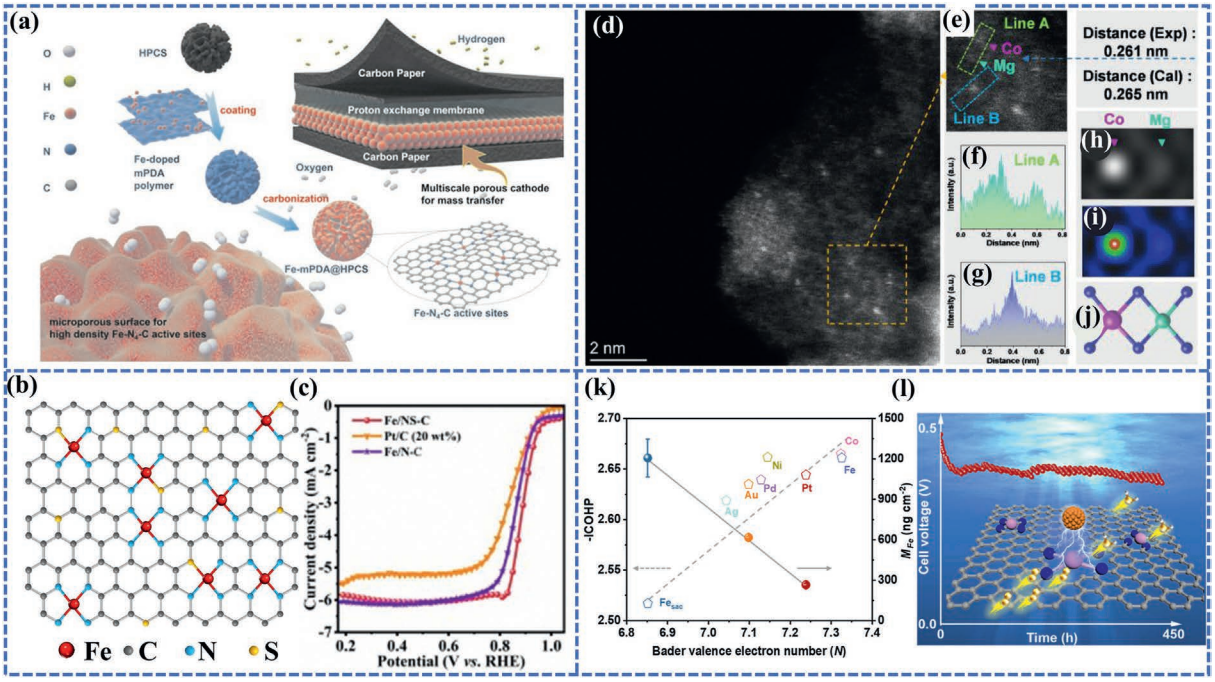


Fig. 5. (a) Schematic of Fe-mPDA@HPCS cathode structure with high-efficiency mass transfer. Reproduced with permission [82]. Copyright 2021, Wiley. (b) Proposed the possible structure of Fe/NS-C. (c) ORR polarization curves. Reproduced with permission [85]. Copyright 2023, Elsevier. (d, e) HAAFF-STEM images. (f, g) Acquired HAADF-STEM intensity line profiles. (h, i) Simulated Mg-Co HAADF-STEM image. (j) Proposed Mg-N-Co moiety in Mg-Co. Reproduced with permission [86]. Copyright 2023, Elsevier. (k) Linear correlation between -ICOHP and Bader valence electron number (N) in different single atom particle catalyst systems (left) and the dissolved Fe content for Fesac, Au-Fesac, and Pt-Fesac (right). (l) Long-term stability test at a constant current density of 0.1 A/cm^2. Reproduced with permission [87]. Copyright 2023, American Chemical Society.

challenge. Wang *et al.* [86] developed a Mg-Co dual-atom catalyst *via* a pyrolysis-impregnation-pyrolysis method, featuring densely populated active sites that significantly enhanced both ORR activity and DMFC performance in acidic media. As shown in Fig. 5d, HAADF-STEM image revealed Mg-Co dual sites, with brighter spots corresponding to Co atoms due to the higher atomic number compared to Mg. Atomic-resolution images (Fig. 5e) and intensity line profiles (Figs. 5f and g) further confirmed the atomic dispersion of metal species without long-range ordering. High-angle annular dark-field scanning transmission electron microscopy (HAADF-STEM) simulations suggested the possible presence of Mg-N_2-Co configurations in the dual-site structure (Figs. 5h and i). Simulation and experimental results deduced the possible a Mg-N_2-Co moiety in Mg-Co atomic pairs (Fig. 5j). The Mg-Co-based DMFC achieved a peak power density of 200 mW/cm^2 and exhibited negligible performance decay after 12 h of operation in a 10 mol/L methanol solution at 80 °C. Precise engineering of local coordination environments enables the rational design of high-performance catalytic systems.

Research on M-N-C catalysts has predominantly emphasized activity and selectivity, with comparatively less attention given to the electrochemical dissolution of metal sites. This is particularly concerning since metal leaching not only contaminates the electrolyte but also degrades active sites, ultimately leading to performance degradation. Although interactions between metal nanoparticle and single atom have been shown to enhance the stability of single-atom catalysts and mitigate metal leaching, the underlying stabilization mechanisms remain poorly understood. Herein, Gao *et al.* [87] proposed and demonstrated a universal mechanism by which metal nanoparticles suppress the dissolution of Fe single atom sites. As illustrated in Fig. 5k, the projected crystal orbital Hamilton population (-pCOHP) was employed to quantitatively evaluate the strength of Fe-N bonds based on its negative values. A positive linear correlation was observed between the integrated negative of the -pCOHP (-ICOHP) and N values, a higher N value corresponds to greater electron density at Fe sites and lower Fe oxidation states, while a higher -ICOHP value indicates stronger Fe-N bonds, thereby inhibiting demetalation. This correlation confirms that metal nanoparticles act as electron donors, enhancing Fe-N bond strength by increasing electron density at FeN_4 centers and thus mitigating Fe dissolution. Electrochemical results revealed a 78 % reduction in Fe dissolution with the nanoparticle-decorated Fe single-atom catalyst, enabling continuous DMFC operation for 430 h at a constant current density of 0.1 A/cm^2 (Fig. 5l).

Through strategies such as confinement engineering, optimization of the coordination micro-environment, increased active site density, and suppression of demetalation, significant progress has been made in the intrinsic activity of catalysts. However, the inherently high surface energy of monodisperse site catalysts still readily leads to migration and aggregation phenomena. Coupled with the generally low metal loading in such catalysts, these issues severely restrict the accessibility and effective exposure of active sites. Furthermore, the dynamic changes in active site structure during catalytic reactions and the difficulties in characterization add to the complexity of understanding structure-activity relationships. Therefore, achieving simultaneous improvements in both stability and metal loading while maintaining high activity remains a fundamental challenge in the development of single-atom catalysts.

3.3. Electronic structure tailoring

The electrocatalytic activity of materials is primarily governed by the surface electronic structure. Typically, the electronic structure of catalysts can be effectively optimized by regulating the composition, defects, and heterostructures. Such electronic structure modulation strategies enable precise adjustment of the electron states, band structure, and surface adsorption capacity of

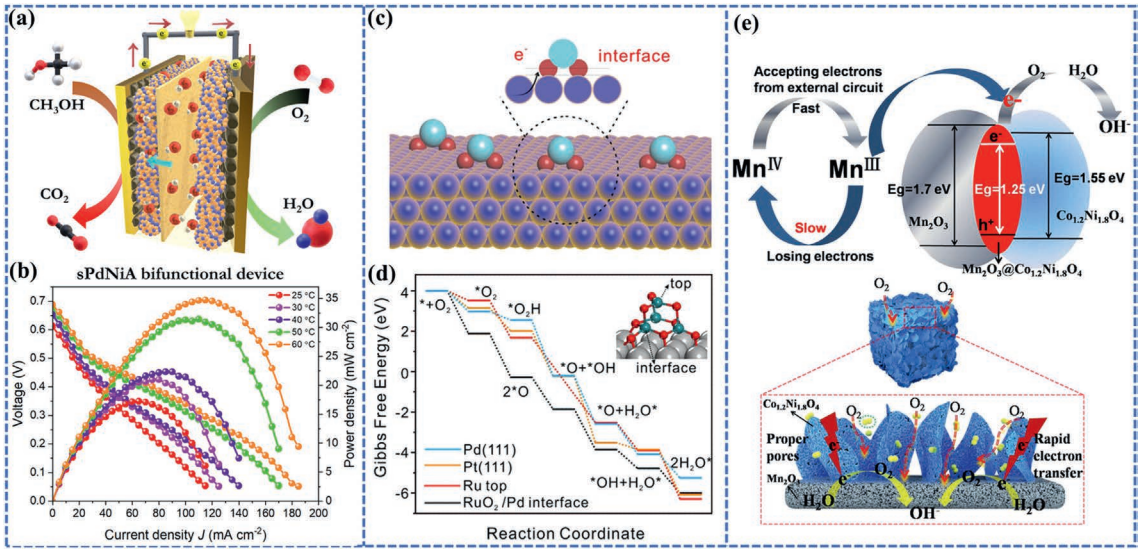


Fig. 6. (a) Schematic representation of the DMFC assembled with the sPdNiA as bifunctional electrodes. (b) Polarization curves of the DMFC at various operating temperatures. Reproduced with permission [100]. Copyright 2023, American Chemical Society. (c) Electron transfer model on RuO_2/Pd(111) interface. (d) Reaction free energy diagram of ORR at different catalytic sites. Reproduced with permission [101]. Copyright 2021, Wiley. (e) Schematic of ORR mechanism for the enhanced electrocatalytic activity of the Mn_2O_3@$Co_{1.2}Ni_{1.8}O_4$. Reproduced with permission [106]. Copyright 2018, American Chemical Society.

catalysts. For instance, approaches including heteroatom doping, strain engineering, alloying, and heterointerface construction have become critical pathways for optimizing electronic structures and enhancing catalytic performance [88–91].

Carbon-based materials are widely studied as ORR electrocatalysts due to the high surface area, low cost, and tunability. However, the intrinsic activity is limited and often requires modification. Heteroatom doping, particularly with N, effectively tunes the morphology, electronic structure, and chemical properties of carbon catalysts. The electronegativity difference may induce charge redistribution, break the electrical neutrality of the carbon matrix and creating charged active sites that promote O_2 adsorption and reduction [92]. Beyond the catalytic role, carbon materials also function as excellent catalyst supports. Graphene is a highly conductive carbon allotrope ideal for framework materials with excellent thermal and electrical conductivity. Farzaneh *et al.* [93] hydrothermally synthesized a novel three-dimensional (3D) mesoporous N-doped reduced graphene oxides (NRGOs) with tunable N content (1.0 %–4.7 %) by controlling melamine/graphene oxide ratios. It was found that N-doping activates π-electrons to enhance low-potential ORR, while pyridinic-N boosts high-potential ORR *via* lone electron pairs. Integrating synergistic heteroatoms can also adjust spin density and charge polarization to enhance catalytic performance. Liu *et al.* [94] reported a 3D porous carbon nanosphere doped with O/N atoms, with diameters below 200 nm and specific surface area exceeding 659 m^2/g, which displayed similar E_{onset} and $E_{1/2}$ compared to commercial 40 wt% Pt/C.

Alloying has attracted significant research interest due to its ability to alter the local electronic environment of metals and induce electronic structure reconstruction. Varying alloy compositions lead to distinct electronic and physicochemical properties, which in turn yield diverse catalytic performances. Current design of alloy catalysts focuses on composition optimization, size control, morphology engineering, and structural design [95–97]. Guided by these strategies, researchers have performed systematic and in-depth studies on alloy catalysts. Introducing transition metals into binary or multicomponent alloys can effectively modulate electronic and ligand effects. Gavidia *et al.* [98] synthesized various carbon-supported Pd-based alloys (PdFe, PdIr, and PdFeIr) *via* borohydride method with precisely controlled compositions. The results demonstrated that the charge transfer from Fe/Ir to Pd played a pivotal role in performance enhancement. Li *et al.* [99] employed an "activity-assisted" strategy to synthesize branched one-dimensional PdBiAu alloy nanochains (size < 6.5 nm) with abundant interfaces. The d-band center of Pd significantly downshifted due to the electronic modulation by adjacent Bi/Au species, weakening the adsorption strength of oxygen intermediates. Benefiting from the synergistic effects, including rich surface defects, lattice strain, optimized d-band center, enhanced methanol tolerance and charge transfer capability, the DFMCs modified with $Pd_{0.60}Bi_{0.35}Au_{0.05}$/C catalyst achieved remarkable power densities of 140.1 and 112.4 mW/cm^2 under 6 mol/L methanol solution when operating in pure O_2 and air atmospheres, respectively. To overcome the kinetic limitations of Pd, Sathyaseelan *et al.* [100] incorporated oxyphilic Ni atom into Pd, successfully synthesizing a sphere-like PdNi alloy (sPdNiA). The incorporation of Ni into the Pd lattice facilitates electron transfer from Ni to Pd, leading to a downshift of the d-band center due to the alloying effect, which confirms the strain effect induced by doping. Fig. 6a illustrated the schematic configuration of a DMFC employing sPdNiA as a bifunctional catalytic layer. As the operating temperature increases, the reaction kinetics accelerate significantly, resulting in a notable improvement in open-circuit voltage and peak power density, reaching 0.68 V and 34 mW/cm^2 at an operating temperature of 60 °C, respectively (Fig. 6b).

Enhanced catalytic performance through interface engineering mainly results from strong metal-support interactions. Downsizing metal components from nano- to atomic-scale allows precise tuning of metal-oxide interfacial effects. Lyu *et al.* [101] reported a two-dimensional (2D) RuO_x/Pd nanosheet featuring atomically dispersed interfaces that significantly enhance metal-oxide interactions. As shown in Fig. 6c, electron transfer from the Pd(111) surface to RuO_x/Pd interface resulted in electron enrichment at the interface, leading to the formation of a dual-end adsorption configuration for O_2. Free energy theoretical calculations further revealed that the optimal O_2 adsorption configuration transformed into one oxygen atom adsorbed at the interfacial Ru site while the other bound to an adjacent Pd site after the formation of RuO_2/Pd(111) interface (Fig. 6d). The dense RuO_x/Pd interface effectively pro-

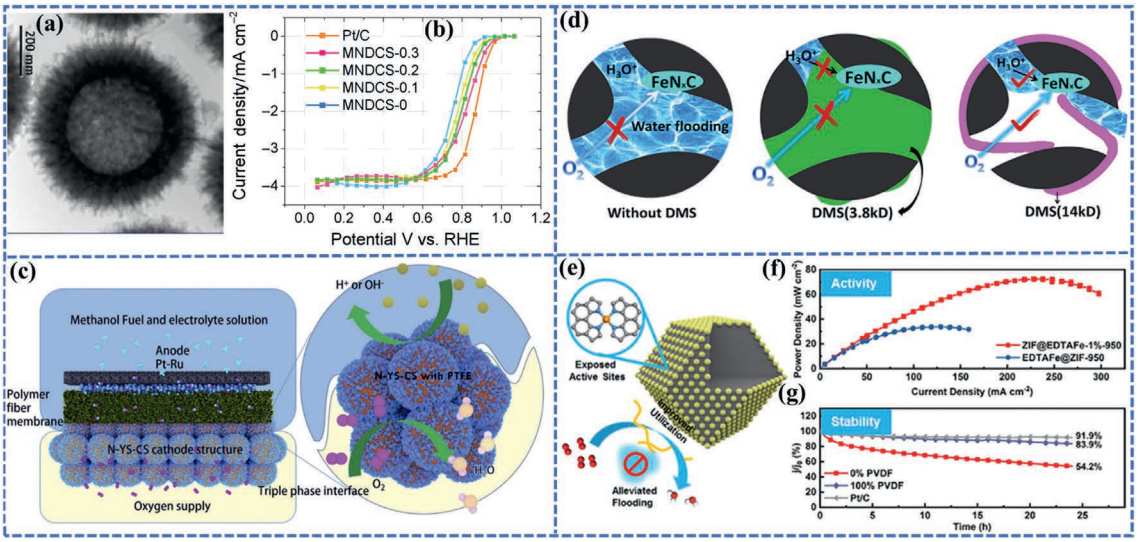


Fig. 7. (a) HAADF-STEM of MNDCS-0.3. (b) ORR polarization curves. Reproduced with permission [107]. Copyright 2020, Wiley. (c) Schematic of the triple-phase interface with N-YS-CS hydrophobic cathode structure. Reproduced with permission [108]. Copyright 2017, Elsevier. (d) Scheme of the microstructure for Fe/N/C cathodes. Reproduced with permission [110]. Copyright 2017, American Chemical Society. (e) Schematic of structural advantages. (f) Power density curves of DMFCs. (g) Short-term stability tests of DMFCs at 100 mA/cm^2. Reproduced with permission [111]. Copyright 2021, American Chemical Society.

moted O_2 activation, O-O bond cleavage, and intermediate conversion processes. CeO_x exhibits abundant surface oxygen species, excellent oxygen storage capacity, and variable valence states, which collectively contribute to its enhanced catalytic performance. As demonstrated by Wang *et al.* [102], the improved activity of PtMo-CeO_x composite primarily stems from the ligand effect and synergistic interactions between Mo and CeO_x nanoparticles. Leveraging the electronic modulation effect of low-electronegativity Ce on Pt and the catalytic effect of CeO_2, Wan *et al.* [103] introduced Ce as a secondary component to tailor the electronic structure of Pt while constructing PtCe-CeO_2 heterointerfaces to enhance reaction kinetics. The heterogeneous interaction between PtCe and CeO_2 facilitated the spontaneous electron donation from Ce to Pt, thereby enhancing the ORR kinetics.

Wang *et al.* [104] synthesized a Fe-urea-formaldehyde resins carbon/MnO_2 composite (Fe-UFC/MnO_2) *via* an *in-situ* redox approach. The resulting Fe-N_x moieties function as effective electrocatalytic active sites. Moreover, Fe incorporation narrows the band gap, promotes the conversion of Mn^{3+} to Mn^{4+}, and directly supplies free electrons to oxygen-adsorbed species, significantly enhancing ORR efficiency. Liu *et al.* [105] prepared bimetallic $NiCo_2O_4$ with 3D dandelion-like (DL) and flower-like (FL) morphologies *via* a facile hydrothermal method. Electrochemical tests indicated electron transfer numbers of 3.97 and 3.91 under alkaline conditions, respectively. DMFC performance improved considerably with increasing operating temperature, reaching maximum power densities of 151 and 114 mW/cm^2 at an operating temperature of 65 °C when assembled with $NiCo_2O_4$-DL and $NiCo_2O_5$-FL, respectively. Mechanistic studies revealed that Co^{3+} acts as an electron donor, directly supplying excited electrons to O_2 for reduction, while Co^{4+} serves as an electron acceptor from the external circuit and is reduced to Co^{3+}, establishing an efficient electron exchange process. In addition, Liu *et al.* [106] developed a novel Mn_2O_3@$Co_{1.2}Ni_{1.8}O_4$ hybrid by decorating ultrathin and highly conductive $Co_{1.2}Ni_{1.8}O_4$ nanosheets onto Mn_2O_3 surfaces. The hybrid exhibited exceptional methanol tolerance even in high-concentration methanol solution and delivered a remarkable power density of 70.5 mW/cm^2 at near room temperature. As shown in Fig. 6e, the enhanced electrocatalytic performance primarily stems from the narrow bandgap of hybrid material, which facilitates electron transition from the valence band to conduction band.

Optimizing the electronic structure of catalysts through strategies such as doping, alloying, and heterostructure engineering serves as a core approach to enhance catalytic performance by modulating the charge distribution and band structure of active sites. This method offers significant advantages, including effectively reducing reaction energy barriers, optimizing the adsorption/desorption behavior of intermediates, and enhancing intrinsic activity and selectivity. Nevertheless, this strategy still faces multiple challenges, such as the complexity of electronic modulation mechanisms, difficulties in precisely controlling doping sites and concentrations, susceptibility to phase separation and component segregation, as well as insufficient interfacial stability and charge transfer efficiency.

3.4. Surface and interface micro-environment engineering

Traditional catalyst design has primarily focused on electronic structure optimization, geometric structure modulation and component engineering. However, as a typical electrode-electrolyte interfacial reaction, the catalytic performance of ORR is profoundly influenced by the macro- and micro-environment at the interface, including factors such as pore structure, surface geometry, hydrophilicity/hydrophobicity, and the degree of active site exposure. These strategies collectively enhance reaction kinetics and structural stability by improving the effective specific surface area, electrical conductivity, mass transport efficiency, electronic structure, interfacial free energy, as well as the density and accessibility of active sites.

Porous carbon offers a high surface area and abundant pore structures, which facilitate mass transfer and increase the accessibility of active sites. However, conventional synthesis methods typically yield mesoporous carbon with limited pore size, large particles (up to micrometers), and a tendency to aggregate, all of which restrict mass transport in fuel cell applications. As shown in Fig. 7a, Shu *et al.* [107] utilized N-rich *m*-phenylenediamine to modulate N active sites and pore structure during the synthesis of mesoporous N-doped carbon spheres (MNDCS). The incorporation of *m*-phenylenediamine effectively modulated precursors nucleation, with the surface structure directly dependent on loading amount. The surface/interface of carbon spheres exhibited abundant functional N species (~6.5 wt%), predominantly pyrrolic

N and pyridinic N species. The optimized micro/mesoporous ratio combined with enhanced N-containing species significantly improved the ORR activity. The MNDCS-0.3 sample (30 wt% *m*-phenylenediamine) achieved a high $E_{1/2}$ of 0.81 V (Fig. 7b). Due to electrode structural constraints and prolonged operation, cathode water flooding progressively worsens, significantly impairing catalyst activity and overall fuel cell performance. This issue underscores the need to construct robust oxygen transport channels tailored for ORR. Shu *et al.* [108] synthesized N-doped yolk-shell carbon spheres (N-YS-CS) with a distinctive core-shell structure, featuring precisely controlled mesoporous surfaces and well-defined core-shell boundaries. Fig. 7c illustrated the membrane electrode assembly in which the PTFE-treated N-YS-CS exhibited high hydrophobicity and flexibility, making it an ideal hydrophobic cathode material. The mesoporous framework of N-YS-CS effectively accommodated hydrophobic agents and formed robust hydrophobic channels within the structure, resulting in a remarkable power output of 142 mW/cm^2 at an operating temperature of 60 °C.

Xu *et al.* [109] developed a microwave-assisted method to rapidly synthesize Fe-doped ZIF-8 precursor, which was further etched with NH_3 under a protective atmosphere to obtain the M_{15}-FeNC-NH_3 catalyst with a hierarchical micro/mesoporous structure. NH_3 etching treatment not only generated new micropores but also expanded some existing micropores into mesopores, while simultaneously increasing the specific surface areas of micropores and mesopores to 749.9 and 554.6 m^2/g, respectively. The interconnected porous network facilitated efficient mass transport of reactants, enabling the resulting DMFC to achieve a peak power density of 61 mW/cm^2 and maintain 95.6 % voltage retention after 24 h with a 0.5 mol/L methanol solution. Although catalytic active sites are typically located within micropores, these pores are highly susceptible to water flooding, which obstructs oxygen diffusion to the active sites and disrupts the three-phase interface. Wang *et al.* [110] introduced hydrophobic dimethyl silicone oil (DMS) as an additive into Fe/N/C catalyst to create a microporous environment that balances hydrophobicity and mass transfer. When the molecular weight of DMS reached 14 kDa, its distribution within the micropores was optimally regulated, effectively mitigating water flooding (Fig. 7d). Polarization curves revealed that DMFC performance initially improved and then declined with increasing DMS molecular weight, peaking at 14 kDa. Under this optimized condition, the DMFC achieved a peak power density of 102 mW/cm^2 using a 3 mol/L methanol solution, matching the performance of Pt/C-based DMFC.

In practical applications of Fe-N-C catalyst, a significant portion of inactive FeN_x sites is embedded deep within the carbon matrix, increasing mass transport resistance and limiting active sites utilization. As shown in Fig. 7e, Xu *et al.* [111] adopted a size-confinement strategy to anchor EDTA-Fe groups on the external surface of ZIF-8, followed by pyrolysis to obtain ZIF@EDTAFe-1 %–950. The resulting material features exposed FeN_4 sites within an epitaxial growth layer. Electrochemical analysis indicated an exceptional active site utilization efficiency of 59.6 %. The highly accessible Fe-N-C configuration, combined with optimized mass transport, enabled the DMFC to reach a peak power density of 71 mW/cm^2 at 0.5 mol/L methanol solution (Fig. 7f). Additionally, PVDF modification of the catalyst layer formed robust hydrophobic channels around the active sites, effectively mitigating flooding. This configuration demonstrated outstanding durability, maintaining 83.9 % voltage retention after 24 h of operation at 100 mA/cm^2 (Fig. 7g).

Surface and interface micro-environment engineering effectively enhances catalytic performance by modulating the local physicochemical environment around active sites. The advantages are primarily demonstrated through the construction of hierarchical pore channels, optimization of interfacial electronic structures, and regulation of hydrophilicity/hydrophobicity, which collectively improve reaction mass transfer, increase the accessibility of active sites, and enhance reaction selectivity, thereby significantly boosting catalytic efficiency and stability. However, this strategy still exhibits certain limitations. For instance, precise control of the microenvironment often relies on complex multi-step synthesis, posing challenges for scalable production and reproducibility. Moreover, the dynamic evolution mechanisms of the micro-environment under practical operating conditions remain unclear, and current characterization techniques are inadequate for real-time resolution of multiphase interfacial processes, hindering in-depth understanding of structure-activity relationships and rational design.

3.5. Additional modulation approaches

The activity of catalysts can be effectively modulated through multi-scale strategies ranging from macro to micro levels, encompassing various dimensions such as morphology, pore structure, particle size, phase composition, surface and interface modification, active site micro-environments, and electronic structure. The mechanisms of strain effects, defect engineering, phase transformation, and ensemble effects on electrocatalytic activity are systematically summarized, with their practical applications discussed in this section.

Tremendous works have demonstrated that electronic and geometric structures are the key influencing factors that determines catalytic activity [42,112–115]. Meanwhile, the use of highly conductive substrates helps improve the catalytic performance of precious metals by reducing resistance-induced polarization losses. For instance, further surface modification of carbon nanotube (CNT) can strengthen interaction with precious metals, thereby preventing the detachment, aggregation, and dissolution of active species [116]. Although defect formation on CNT promotes the growth of Pt nanoparticles, effective methods for precisely controlling such defects remain scarce. To address this, Hu *et al.* [117] employed plasma treatment on N-doped CNT, which generated abundant surface defects that facilitated the uniform dispersion and stabilization of Pt nanoparticles (p-Pt@p-NCNT). Meanwhile, plasma reduction resulted in Pt nanoparticles with a lower proportion of surface atoms in high oxidation states. As illustrated in Fig. 8a, p-Pt@p-NCNT consisted of Pt nanoparticles supported on bamboo-shaped NCNT featuring numerous defects. Pt 4f X-ray photoelectron spectroscopy (XPS) spectrum (Fig. 8b) and DFT calculations further revealed that plasma-treated surface provided favorable sites for Pt nanoparticles attachment, inducing strong electronic coupling between Pt and NCNT support. This modification optimized the surface oxidation state of Pt, thereby lowering the energy barrier of rate determining step in ORR. Consequently, the p-Pt@p-NCNT-based DMFC achieved a high peak power density of 81.9 mW/cm^2 at an operating temperature of 80 °C. Liu *et al.* [118] introduced trace amounts of Ru into Co nanoclusters, resulting in atomically dispersed Ru on Co. Benefiting from the ligand and strain effects, the catalyst demonstrated significantly enhanced ORR activity, achieving a $E_{1/2}$ of 0.908 V and high selectivity toward the 4e$^-$ pathway. When tested in fuel cell, the catalyst demonstrated a 60 % improvement in performance compared to commercial Pt/C, highlighting the strong potential for practical fuel cell applications.

Currently, systematic studies on hollow-structured PtM (M = transition metal) alloy catalysts remain scarce, especially in terms of the controllable synthesis of diverse alloy phases and architectures, as well as the understanding of how compositional and morphological synergies govern electrocatalytic performance. Through precise adjustment of precursor ratios and pyrolysis temperature, Fan *et al.* [119] realized gradient composition control and ordered atomic arrangement in PtNi alloy nanotube. Lattice

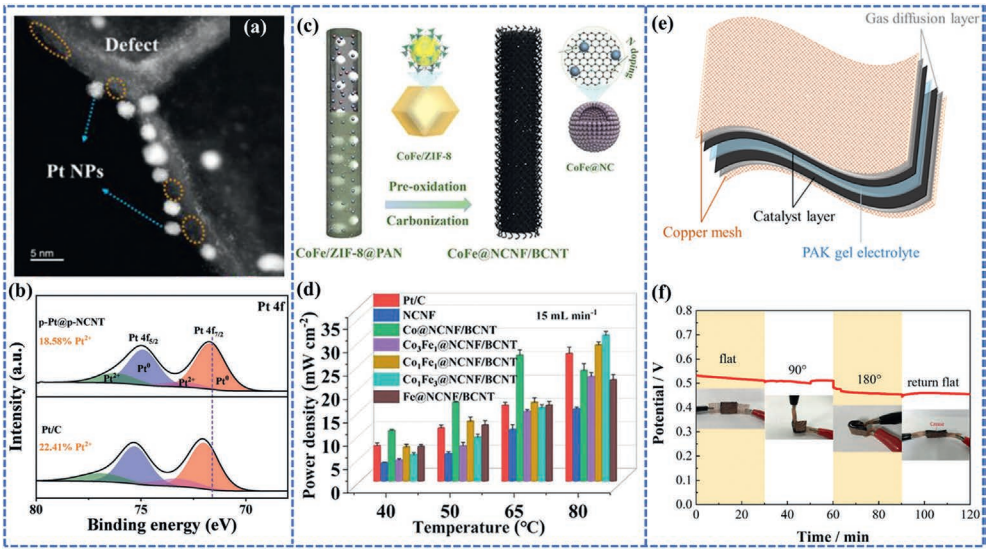


Fig. 8. (a) Aberration-corrected HRTEM. (b) high-resolution XPS spectra of Pt 4f. Reproduced with permission [117]. Copyright 2023, Wiley. (c) Schematic of the CoFe@NCNF/BCNT synthesis. (d) The peak power densities obtained at different operating temperatures. Reproduced with permission [121]. Copyright 2023, Elsevier. (e) Structure diagram of flexible DMFC. (f) The electrochemical performance of DMFC under consecutive bending from flat to 180°. Reproduced with permission [12]. Copyright 2021, American Chemical Society.

contraction effect induced by Ni-doping (wall thickness: 19 nm) resulted in optimal electrocatalytic performance at a Ni/Pt atomic ratio of 2.2. The catalyst retained 91.2 % of its initial mass activity after 10,000 accelerated durability test cycles. Zou *et al.* [120] systematically explored the structural evolution from disordered PtNi alloys to ordered PtNi intermetallic compounds and its impact on catalytic behavior. The ordered PtNi intermetallic nanoparticles demonstrated markedly improved ORR activity, durability, and methanol tolerance compared to the disordered counterparts.

The metal ion ratio in precursors determines the composition and electronic structure of the resulting alloy nanoparticles. As shown in Fig. 8c, our group developed a nanoengineering strategy to synthesize a series of CoFe alloy catalysts confined in N-doped carbon nanofibers (NCNF) and bamboo-like carbon nanotubes (BCNT) by pyrolyzing precursors with precisely controlled Co/Fe molar ratios (1:0, 3:1, 1:1, 1:3, 0:1) [121]. Owing to optimized N coordination, precisely tuned alloy composition, and strong electronic coupling effects, the DMFCs assembled with Co_1Fe_1@NCNF/BCNT and Co_1Fe_3@NCNF/BCNT demonstrated high power densities of 29.10 and 31.11 mW/cm^2 when operating at an operating temperature of 80 °C, respectively (Fig. 8d). Ultra-thin 2D materials have garnered growing research attention owing to their distinctive performance advantages. Nevertheless, synthetic strategies for ultrathin 2D Pd-based nanomaterials with multicomponent compositions are still scarcely reported. In an innovative approach, Zhao *et al.* [122] developed a visible-light-induced templating method to fabricate quaternary PdAuBiTe alloy nanosheets (PdAuBiTe ANSs) with a thickness of approximately 5 nm. The prepared catalyst demonstrated exceptional electrocatalytic performance, which can be attributed to its abundant edge and surface defects, lattice strain effects, optimized d-band center, and ensemble effects. These advantages ultimately enabled the DMFC to achieve remarkable maximum power densities of 235.7 mW/cm^2 (in O_2) and 173.5 mW/cm^2 (in air) at 10 mol/L methanol solution. Conventional DMFC are often hindered by bulky volume, high cost, and severe methanol crossover, which present major obstacles to the development of flexible DMFC devices. As shown in Fig. 8e, Li *et al.* [12] innovatively proposed a flexible DMFC design strategy employing a highly active Fe(Fc)-N/S-C cathode material integrated with a mechanically robust potassium polyacrylate hydrogel (PAK gel) electrolyte. Deformation-discharge tests demonstrated that the assembled flexible DMFC maintained a stable output voltage of approximately 0.458 V even after returning to its flat state (Fig. 8f). This design offers new insights for developing flexible DMFC that combine both low cost and high energy conversion efficiency.

In the modification of electrocatalysts, multiple strategies such as strain effects, defect engineering, phase transformation, and ensemble effects work synergistically to regulate catalytic performance across various dimensions, including electronic structure, coordination environment, crystal phase, and active-site microstructure. Specifically, lattice strain can be introduced to modulate surface electronic structure; unsaturated coordination sites can be constructed to enhance local charge density and reaction activity; structural reconstruction can be utilized to expose highly active crystal facets; and synergistic mechanisms can be employed to promote efficient multi-step reaction processes. However, these strategies still face significant challenges, such as difficulties in precisely controlling defect concentration and distribution, the irreversibility of phase transformation processes, the reliance on precise assembly for complex structures, and the unclear synergistic mechanisms among multiple effects, which represent critical bottlenecks for further development.

4. Conclusions and perspectives

Advances in nanotechnology have opened new opportunities for the design and optimization of electrocatalysts. This review begins with an overview of the fundamental working principles of DMFC and the mechanisms of the ORR, then systematically summarizes recent advances in modification strategies for ORR catalysts. These include methanol tolerance optimization, precise design of active sites, electronic structure modulation, surface/interface micro-environment engineering, and other synergistic methods. Multi-scale strategies, such as core-shell structure, nanoengineering, heteroatom doping, alloying, metal-support interactions, defect engineering, and interface engineering are emphasized, with the mechanisms for improving catalytic activity and methanol tolerance discussed in detail. However, current ORR catalysts still require considerable improvements in structural design and overall performance. The following key challenges remain to be addressed:

(1) The aforementioned activity modulation strategies primarily cover precious metal catalysts, carbon-based materials, single-atom catalysts, alloy catalysts, and metal oxides. For precious metal catalysts, it is necessary to reduce precious metal loading while maintaining catalytic activity and improving methanol tolerance. Carbon-based materials suffer from low activity and poor long-term stability, with the catalytic mechanism of heteroatom doping remaining unclear. Single-atom catalysts require enhanced stability and loading capacity, the ORR activity strongly depends on the M-N-C coordination environment and metal centers, making precise structural control critical. Alloy catalysts encounter issues such as poor synthesis controllability, component segregation, and high precious metal dependence, urgently demanding advanced synthesis techniques and stability enhancement strategies. Additionally, metal oxides exhibit low conductivity, necessitating surface defect/doping engineering, conductive network construction, crystal structure modulation, and interface engineering to synergistically improve both conductivity and ORR activity. Catalyst design aims to achieve high activity, high stability, and low cost simultaneously, yet balancing all three remains challenging. An ideal catalyst should combine high site density to achieve high activity while maintaining a low dissolution rate to ensure long-term stability.

(2) With the advancement of catalytic science, traditional methods have become inadequate in deciphering the complex and non-linear structure-activity relationships between high-dimensional features of catalysts (*e.g.*, chemical composition, morphology, size distribution, coordination environment) and the performance metrics including activity, selectivity, and stability. Recent breakthroughs in characterization techniques, including aberration-corrected transmission electron microscopy (AC-TEM), *in situ* Raman spectroscopy, and *in situ* X-ray absorption fine structure (XAFS) spectroscopy, now allow real-time tracking the coordination environment and valence changes of active sites, providing direct evidence for mechanisms behind ORR activity. DFT calculations complement experiments by revealing adsorption free energy changes of intermediates and electronic properties. Meanwhile, machine learning identifies patterns in data to build predictive models and guide inverse catalyst design, uncovering new mechanisms and shifting research from trial-and-error to precision approaches. Together, these integrated techniques deepen understanding of catalytic processes and establish a robust foundation for designing next-generation high-performance catalysts.

(3) The ORR catalysts developed in laboratories often demonstrate superior intrinsic activity compared to commercial Pt/C in three-electrode system, primarily due to the idealized testing environment (including high O_2 solubility, ultrathin catalyst layers, and efficient mass transport conditions), which maximizes active site utilization and optimizes ion/electron transport pathways. However, in practical DMFC operation, complex gas-liquid-solid interfaces, mass transport resistance caused by thicker catalyst layers, electron/proton conduction imbalance, and material degradation during long-term operation (*e.g.*, support corrosion and active metal leaching) significantly limit the practical performance of electrocatalysts. In contrast, precious metal catalysts still dominate the fuel cell field due to the mature electrode engineering technology. This performance gap highlights the critical technical challenges in transitioning from intrinsic material properties to device-level engineering applications. Three-electrode measurements are essential in basic research for rapid material screening and mechanistic studies. In applied research and development, integrated testing of flexible/wearable DMFC is crucial to evaluating device performance, system compatibility, and practical engineering challenges.

CRediT authorship contribution statement

Shiquan Guo: Writing – original draft, Writing – review & editing, Investigation, Conceptualization. **Fei Chen:** Formal analysis, Methodology. **Congju Li:** Writing – review & editing, Supervision, Funding acquisition.

Declaration of competing interest

The authors declare that they have no known competing financial interests or personal relationships that could have appeared to influence the work reported in this paper.

Acknowledgments

This work is supported by the Beijing Municipal Natural Science Foundation (No. 2252043), the National Natural Science Foundation of China (No. 52170019), the Fundamental Research Funds for the Central Universities (No. 06500100), and the "Ten Thousand Plan"-National High-level personnel of special support program.

Supplementary materials

Supplementary material associated with this article can be found, in the online version, at doi:10.1016/j.cclet.2026.112408.

References

[1] F. Creutzig, Nature 606 (2022) 460–462.
[2] M. Murunga, C. Macleod, G. Pecl, Nat. Clim. Change 14 (2024) 126–133.
[3] K. Yuan, T.T. Zhang, X.M. Xie, et al., J. Cleaner Prod. 414 (2023) 137590.
[4] Y.Q. Yang, S. Bremner, C. Menictas, M. Kay, Renew. Sustain. Energy Rev. 167 (2022) 112671.
[5] F. Belaïd, A. Al-Sarihi, R. Al-Mestneer, Renew. Energy 205 (2023) 534–542.
[6] M.L. Yue, H. Lambert, E. Pahon, et al., Renew. Sustain. Energy Rev. 146 (2021) 111180.
[7] Z.T. Li, X.T. Xu, X.R. Sheng, et al., ACS Nano 15 (2021) 12535–12566.
[8] Y.D. Lei, Z.L. Wang, D.Y. Wang, et al., Nat. Clim. Change 13 (2023) 693–700.
[9] X. Zhao, H. Zhou, V.S. Sikarwar, et al., Energy Environ. Sci. 10 (2017) 1885–1910.
[10] O.W. Sheng, C.B. Jin, X.F. Ding, et al., Adv. Funct. Mater. 31 (2021) 2100891.
[11] Y. Wang, Y.H. Pang, H. Xu, A. Martinez, K.S. Chen, Energy Environ. Sci. 15 (2022) 2288–2328.
[12] X.H. Li, T.T. Chao, Y.E. Duan, et al., ACS Sustainable Chem. Eng. 9 (2021) 15138–15146.
[13] D.F. Chen, P.C. Pei, Y.H. Li, et al., Energy Convers. Manage. 261 (2022) 115651.
[14] D.X. Xie, S.J. Hu, D.H. Teng, et al., Chem. Eng. J. 457 (2023) 141310.
[15] H. Chen, J. Song, X. Long, et al., Appl. Catal. B 361 (2025) 124643.
[16] M.F.R. Hanifah, J. Jaafar, M.H.D. Othman, et al., Electrochim. Acta 403 (2022) 139608.
[17] Ş. Neaţu, F. Neaţu, I.M. Chirica, et al., J. Mater. Chem. A 9 (2021) 17065–17128.
[18] K.L. Wang, P.C. Liu, M.Z. Wang, et al., Chin. Chem. Lett. 36 (2025) 110532.
[19] Z.L. Wu, Q.H. Yang, Y. Liu, et al., ACS Catal. 12 (2022) 3063–3082.
[20] J. Liu, J. Zhao, H.Q. Wei, Q. Zhu, Y. Li, Energy Convers. Manage. 302 (2024) 118128.
[21] F.S. Nanadegani, B. Sunden, Int. J. Hydrogen Energy 48 (2023) 32875–32942.
[22] D. Gerteisen, J. Power Sources 195 (2010) 6719–6731.
[23] Y.H. Zuo, W.C. Sheng, W.Q. Tao, Z. Li, J. Mater. Sci. Technol. 114 (2022) 29–41.
[24] S. Zaman, L. Huang, A.I. Douka, et al., Angew. Chem., Int. Ed. 133 (2021) 17976–17996.
[25] Y. Wang, D.S. Wang, Y.D. Li, Adv. Mater. 33 (2021) 2008151.
[26] Y.H. He, Q. Tan, L.L. Lu, J. Sokolowski, G. Wu, Electrochem. Energy Rev. 2 (2019) 231–251.
[27] L.M. Dai, Y.H. Xue, L.T. Qu, H.J. Choi, J.B. Baek, Chem. Rev. 115 (2015) 4823–4892.
[28] C.Z. Wan, X.F. Duan, Y. Huang, Adv. Energy Mater. 10 (2020) 1903815.
[29] Y.X. Sun, H.Y. Li, S.Q. Guo, C.J. Li, Chin. Chem. Lett. 35 (2024) 109418.
[30] M.L. Liu, Z.P. Zhao, X.F. Duan, Y. Huang, Adv. Mater. 31 (2019) 1802234.
[31] X.Q. Wang, Z.J. Li, Y.T. Qu, et al., Chem 5 (2019) 1486–1511.
[32] X.L. Tian, X.F. Lu, B.Y. Xia, X.W. Lou, Joule 4 (2020) 45–68.
[33] G. Alemany-Molina, C. Lo Vecchio, V. Baglio, et al., J. Colloid Interface Sci. 691 (2025) 137426.
[34] L.L. Zhang, P.P. Lu, M.M. Yin, et al., Rare Met 44 (2024) 1767–1776.
[35] K. Singh, E.B. Tetteh, H.Y. Lee, T.H. Kang, J.S. Yu, ACS Catal. 9 (2019) 8622–8645.
[36] H. Xu, H.Y. Shang, C. Wang, Y.K. Du, Adv. Funct. Mater. 30 (2020) 2000793.
[37] C. Li, N. Clament Sagaya Selvam, J.Y. Fang, Nano-Micro Lett. 15 (2023) 83.
[38] S.S.A. Shah, T. Najam, M.S. Bashir, et al., Small 18 (2022) 2106279.

[39] T. Najam, S.S.A. Shah, S. Ibraheem, et al., Energy Storage Mater. 45 (2022) 504–540.
[40] J.Y. Zhao, J. Lian, Z.X. Zhao, X.M. Wang, J.J. Zhang, Nano-Micro Lett. 15 (2022) 19.
[41] H.X. Zhong, M.C. Wang, G.B. Chen, R.H. Dong, X.L. Feng, ACS Nano 16 (2022) 1759–1780.
[42] H.D. Xu, J. Yang, R.Y. Ge, et al., J. Energy Chem. 71 (2022) 234–265.
[43] W.Y. Zhang, S.Y. Yi, Y.H. Yu, et al., J. Mater. Chem. A 12 (2024) 87–112.
[44] M.Y. Chen, J.Q. Guan, Adv. Funct. Mater. 35 (2025) 2423552.
[45] Y.F. Guo, L.L. Zhao, N. Zhang, et al., Energy Storage Mater. 70 (2024) 103556.
[46] X. Wu, Q. Yan, H. Wang, et al., Adv. Funct. Mater. 34 (2024) 2404535.
[47] J.J. Huo, Y.H. Dou, C. Wu, et al., Adv. Mater. 37 (2025) 2416483.
[48] Z. Zhang, P.Z. Liu, Y.H. Song, et al., Adv. Sci. 9 (2022) 2204297.
[49] R.Y. Ge, S.H. Yu, Y.W. Li, et al., Adv. Mater. 37 (2025) 2503223.
[50] Z.W. Zhang, H.H. Jin, J.W. Zhu, et al., Carbon 161 (2020) 502–509.
[51] H.J. Shen, T.J. Thomas, S.A. Rasaki, et al., Electrochem. Energy Rev. 2 (2019) 252–276.
[52] S.L. Li, L. Shi, Y.J. Guo, et al., Chem. Sci. 15 (2024) 11188–11228.
[53] Z.Q. Zhu, Z.J. Li, Z.H. Liu, et al., Small Methods 10 (2026) 2500411.
[54] M.A. Ud Din, M. Idrees, S. Jamil, et al., J. Energy Chem. 77 (2023) 499–513.
[55] C. Lee, C.K. Hwang, J.W. An, et al., Appl. Catal. B 358 (2024) 124371.
[56] Y. Feng, H. Liu, J. Yang, Sci. Adv. 3 (2017) e1700580.
[57] H.F. Zhang, X.Y. Qiu, Y.F. Chen, et al., Small 16 (2020) 1906026.
[58] X.L. Wang, J.W. Li, X.T. Yang, et al., Nano Res. 15 (2022) 7951–7958.
[59] K. Cheng, Z.K. Kou, J. Zhang, et al., J. Mater. Chem. A 3 (2015) 14007–14014.
[60] X. Tong, J.M. Zhang, G.X. Zhang, et al., Chem. Mater. 29 (2017) 9579–9587.
[61] D. Lee, S. Gok, Y. Kim, et al., ACS Appl. Mater. Interfaces 12 (2020) 44588–44596.
[62] Y. Zhang, B.L. Huang, G. Luo, et al., Sci. Adv. 6 (2020) eaba9731.
[63] S. Kim, J.E. Park, W. Hwang, Y.H. Cho, Y.E. Sung, Appl. Catal. B 209 (2017) 91–97.
[64] C.J. Hou, W.J. Yuan, Y.J. Zhang, et al., Fuel 379 (2025) 133111.
[65] Q. Tan, T. Qu, C.Y. Shu, et al., ACS Sustainable Chem. Eng. 7 (2019) 17145–17153.
[66] Q.R. Shi, Y.H. He, X.W. Bai, et al., Energy Environ. Sci. 13 (2020) 3544–3555.
[67] S.K. Singh, K. Takeyasu, J. Nakamura, Adv. Mater. 31 (2019) 1804297.
[68] J. Zhang, J.J. Zhang, F. He, et al., Nano-Micro Lett. 13 (2021) 65.
[69] W.Q. Song, C.X. Xiao, J. Ding, et al., Adv. Mater. 36 (2024) 2301477.
[70] M.M. Liu, L.L. Wang, K.N. Zhao, et al., Energy Environ. Sci. 12 (2019) 2890–2923.
[71] Z.L. Yang, L.Q. Liu, X.B. Rao, et al., Chin. Chem. Lett. 36 (2025) 111440.
[72] J.F. Huang, S. Ajmal, A. Kumar, et al., J. Energy Chem. 101 (2025) 132–155.
[73] M.J. Gong, A. Mehmood, B. Ali, K.W. Nam, A. Kucernak, ACS Catal. 13 (2023) 6661–6674.
[74] I. Martinaiou, A.H.A. Monteverde Videla, N. Weidler, et al., Appl. Catal. B 262 (2020) 118217.
[75] L.Z. Gu, L.H. Jiang, X.N. Li, et al., Chin. J. Catal. 37 (2016) 539–548.
[76] X.T. Zhao, X. Maimaitiyiming, M. Tursun, H. Lin, Fuel 364 (2024) 131089.
[77] D. Sebastián, A. Serov, K. Artyushkova, et al., J. Power Sources 319 (2016) 235–246.
[78] X.Y. Zhang, D.P. Xue, S. Jiang, et al., InfoMat 4 (2022) e12257.
[79] H.G. Huang, K. Shen, F.F. Chen, Y.W. Li, ACS Catal. 10 (2020) 6579–6586.
[80] X.L. Xu, Z.X. Xia, X.M. Zhang, et al., Appl. Catal. B 259 (2019) 118042.
[81] J.W. Shi, H.B. Shao, F. Yang, et al., Chem. Eng. J. 445 (2022) 136628.
[82] C.Y. Shu, Q. Tan, C.W. Deng, et al., Carbon Energy 4 (2022) 1–11.
[83] A. Yu, Y. Yang, Angew. Chem., Int. Ed. 64 (2025) e202424161.
[84] Y. Wang, Y.X. Wang, J. Zhao, et al., ACS Sustainable Chem. Eng. 12 (2024) 6982–6989.
[85] L.F. Cui, J. Hao, Y. Zhang, et al., J. Colloid Interface Sci. 650 (2023) 603–612.
[86] K.W. Wang, H.J. Zou, J.Z. Meng, et al., J. Magnesium Alloys 11 (2023) 1959–1969.
[87] X.B. Gao, Y.C. Wang, W.C. Xu, et al., J. Am. Chem. Soc. 145 (2023) 15528–15537.
[88] Q.J. Niu, B.L. Chen, J.X. Guo, et al., Nano-Micro Lett. 11 (2019) 8.
[89] C.G. Hu, R. Paul, Q.B. Dai, L.M. Dai, Chem. Soc. Rev. 50 (2021) 11785–11843.
[90] C. Kim, F. Dionigi, V. Beermann, et al., Adv. Mater. 31 (2019) 1805617.
[91] K.S. Bejigo, R.A. Raj, S.J. Kim, Sustainable Mater. Technol. 42 (2024) e01153.
[92] L.Z. Liu, G. Zeng, J.X. Chen, et al., Nano Energy 49 (2018) 393–402.
[93] A. Farzaneh, N. Saghatoleslami, E.K. Goharshadi, H. Gharibi, H. Ahmadzadeh, Electrochim. Acta 222 (2016) 608–618.
[94] Y. Liu, T. Zhang, X. Dai, et al., ACS Appl. Nano Mater. 3 (2020) 5139–5148.
[95] L.Y. Gong, J. Liu, Y. Li, et al., Chem. Eng. J. 428 (2022) 131569.
[96] P. Anandha ganesh, D. Jeyakumar, Electrochim. Acta 262 (2018) 306–318.
[97] W.J. Wang, Z.Q. Jiang, X.N. Tian, T. Maiyalagan, Z.J. Jiang, Carbon 201 (2023) 1068–1080.
[98] L.M. Rivera Gavidia, G. García, D. Anaya, et al., Appl. Catal. B 184 (2016) 12–19.
[99] X. Li, K.X. Yao, F.L. Zhao, et al., Nano Res. 15 (2022) 6036–6044.
[100] A. Sathyaseelan, V. Elumalai, K. Krishnamoorthy, A. Sajeev, S.J. Kim, ACS Sustainable Chem. Eng. 11 (2023) 5345–5355.
[101] Z.X. Lyu, X.G. Zhang, Y.C. Wang, et al., Angew. Chem., Int. Ed. 133 (2021) 16229–16236.
[102] P. Wang, H. Cui, C.X. Wang, Chem. Eng. J. 429 (2022) 132435.
[103] Z.Q. Wan, J.Q. Ye, J.Y. Zhang, et al., J. Mater. Chem. A 13 (2025) 9729–9736.
[104] Y.H. Wang, F. Wang, Y. Fang, et al., Appl. Surf. Sci. 496 (2019) 143566.
[105] Y. Liu, C.Y. Shu, Y. Fang, Y.Z. Chen, Y.N. Liu, J. Power Sources 361 (2017) 160–169.
[106] Y. Liu, Y.Z. Chen, S. Li, et al., ACS Appl. Mater. Interfaces 10 (2018) 9485–9494.
[107] C.Y. Shu, Z. Gan, Y.Y. Hou, et al., Energy Environ. Mater. 4 (2020) 81–87.
[108] C.Y. Shu, B. Song, X.D. Wei, et al., Carbon 129 (2018) 613–620.
[109] X.L. Xu, X.M. Zhang, Z.X. Xia, et al., J. Energy Chem. 54 (2021) 579–586.
[110] Y.C. Wang, L. Huang, P. Zhang, et al., ACS Energy Lett. 2 (2017) 645–650.
[111] X.L. Xu, X.M. Zhang, Z.X. Xia, et al., ACS Appl. Mater. Interfaces 13 (2021) 16279–16288.
[112] X.Q. Zheng, Z.C. Wang, Q. Zhou, et al., J. Energy Chem. 88 (2024) 242–251.
[113] P. Basumatary, J.H. Choi, D. Konwar, et al., Small Methods 8 (2024) 2301651.
[114] M.X. Du, D. Li, S.Z. Liu, J.Q. Yan, Adv. Funct. Mater. 33 (2023) 2301527.
[115] Q.Y. Guo, Y. Yang, T.T. Hu, et al., Chin. Chem. Lett. 36 (2025) 110235.
[116] X.L. Zhao, F. Li, R.N. Wang, et al., Adv. Funct. Mater. 27 (2017) 1605717.
[117] T.T. Hu, W.H. Chen, Y.B. Liu, et al., Small 19 (2023) 2304076.
[118] Z. Liu, S.F. Zhou, S.X. Ma, et al., Mater. Today Phys. 17 (2021) 100338.
[119] C.T. Fan, G.L. Wang, L.L. Zou, et al., J. Power Sources 429 (2019) 1–8.
[120] L.L. Zou, J. Fan, Y. Zhou, et al., Nano Res. 8 (2015) 2777–2788.
[121] S.Q. Guo, S.Y. Yu, F. Chen, et al., J. Colloid Interface Sci. 652 (2023) 429–439.
[122] F.L. Zhao, L.R. Zheng, Q. Yuan, et al., Adv. Mater. 33 (2021) 2103383.